Structure
Article

The Bacterial Stressosome: A Modular System that Has Been Adapted to Control Secondary Messenger Signaling

Maureen B. Quin,[1,2,3] John M. Berrisford,[1,3] Joseph A. Newman,[1] Arnaud Baslé,[1] Richard J. Lewis,[1,*] and Jon Marles-Wright[1,*]
[1]Institute for Cell and Molecular Biosciences, Newcastle University, Newcastle upon Tyne, NE2 4HH, UK
[2]Present address: Gortner Laboratory of Biochemistry, University of Minnesota, Saint Paul, MN 55108, USA
[3]These authors contributed equally to this work
*Correspondence: rick.lewis@ncl.ac.uk (R.J.L.), jon.marles-wright@ncl.ac.uk (J.M.-W.)
DOI 10.1016/j.str.2012.01.003

SUMMARY

The stressosome complex regulates downstream effectors in response to environmental signals. In *Bacillus subtilis*, it activates the alternative sigma factor σ^B, leading to the upregulation of the general stress regulon. Herein, we characterize a stressosome-regulated biochemical pathway in *Moorella thermoacetica.* We show that the presumed sensor, MtR, and the scaffold, MtS, form a pseudo-icosahedral structure like that observed in *B. subtilis.* The N-terminal domain of MtR is structurally homologous to *B. subtilis* RsbR, despite low sequence identity. The affinity of the switch kinase, MtT, for MtS decreases following MtS phosphorylation and not because of structural reorganization. Dephosphorylation of MtS by the PP2C type phosphatase MtX permits the switch kinase to rebind the stressosome to reset the response. We also show that MtT regulates cyclic di-GMP biosynthesis through inhibition of a GG(D/E)EF-type diguanylate cyclase, demonstrating that secondary messenger levels are regulated by the stressosome.

INTRODUCTION

The stressosome signaling system was first identified and characterized in the Gram-positive model bacterium *Bacillus subtilis* (Dufour et al., 1996; Chen et al., 2003). Here, the stressosome appears to act as both the sensor and the initiator of the response to environmental stresses, which is mediated by the alternative RNA polymerase sigma factor σ^B (Haldenwang and Losick, 1979; Marles-Wright et al., 2008; Price et al., 2001). Gene clusters encoding stressosome homologs have been found in representatives of most bacterial phyla, from the pathogenic marine bacterium *Vibrio vulnificus,* which can cause fatal septicemia (Horseman and Surani, 2011) to the thermophilic acetogen *Moorella thermoacetica* (Pané-Farré et al., 2005). All species in which stressosome homologs have been identified possess a conserved genetic arrangement, consisting of an upstream module of genes within the operon that encodes proteins equivalent to the Regulator of σ^B proteins (Rsb) of *B. subtilis*: RsbR, RsbS, RsbT, and RsbX. In addition, there is a downstream module comprising a series of genes with differing functions (Pané-Farré et al., 2005). In *B. subtilis*, RsbU, RsbV, RsbW, and σ^B are inserted between the RsbT and RsbX genes.

The RsbR homologs encode a variable N-terminal domain, which may act as a sensor, and a conserved STAS (Sulfate Transport and Anti-anti-Sigma factor) C-terminal domain (Akbar et al., 1997). The gene encoding RsbR is always followed by that for the single STAS domain protein RsbS, which multimerizes with RsbR to form a 1.5 MDa, pseudo-icosahedral complex termed the stressosome (Chen et al., 2003). Consistent with the role of the better conserved STAS domains in protein:protein interactions, it is the C-terminal STAS domain of RsbR that interacts with RsbS to form stressosomes in *B. subtilis* (Marles-Wright et al., 2008). The sequence variability of the N-terminal domains of RsbR is more consistent with a role in sensory perception than as a scaffold (Caffrey et al., 2004). Therefore, the stressosome complex provides a platform for diverse signaling modules to generate a response that is tunable to the magnitude of the signal (Marles-Wright et al., 2008). The subsequent gene in the module encodes a ''switch'' protein kinase, RsbT, the substrates of which are conserved serine (Ser59 in *B. subtilis*) and threonine (Thr171 and Thr205 in *B. subtilis*) residues in RsbS and RsbR, respectively (Gaidenko et al., 1999). RsbT is also part of the stressosome complex (Chen et al., 2003), and, in a mechanism that is so far not understood, its kinase activity is activated upon the perception of a stress signal. RsbT subsequently phosphorylates both RsbR and RsbS, whereupon RsbT dissociates from the stressosome complex (Chen et al., 2003; Yang et al., 1996). On disassociation from the stressosome, RsbT interacts with, and activates, RsbU, a type 2C protein phosphatase (Yang et al., 1996).

In *B. subtilis*, the N-terminal ~120 amino acids of RsbU is a kinase recruitment domain, which mediates the interaction with RsbT that is critical to the σ^B signal transduction cascade (Delumeau et al., 2004), whereas the C-terminal domain provides a catalytic, phosphatase function. The RsbU N-terminal domain is found linked to other effectors in different species. For instance, it is found as a domain within part of hybrid two-component histidine kinase (e.g., in *Paenibacilli*, *Mycobacteria*, and *Oxalobacteraceae*), as a domain in diguanylate cyclases

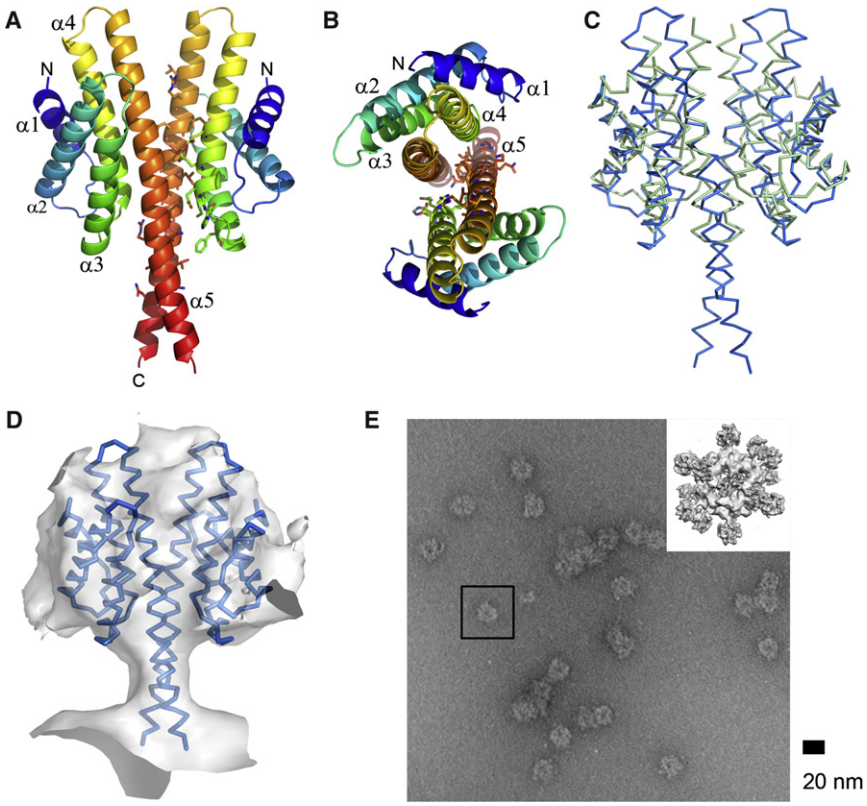

Figure 1. Structure of N-MtR

(A) Cartoon of the overall fold of the N-terminal domain of MtR. The protein structure is color ramped from N terminus (blue) to C terminus (red). Interface residues are shown as sticks for a single chain.

(B) Orthogonal view of (A) down the crystallographic 2-fold dimer axis.

(C) Superimposition of dimers of *N*-RsbR (green) and N-MtR (blue).

(D) Fit of *N*-MtR in the experimental cryo-EM map of the *B. subtilis* stressosome (EMDB: 1555).

(E) Negative stain TEM image of MtR:MtS stressosome complexes. A single isolated complex is highlighted with a black box, with the reconstruction of the *B. subtilis* stressosome shown as an inset for comparison.

from *Methylobacter tundripaludum* and with other conserved domains of unknown function (Pané-Farré et al., 2005).

In *Moorella thermoacetica,* the gene immediately downstream of the homologs of the RsbR-RsbS-RsbT module (orfs *moth_1475-1473*) encodes an RsbX-like PP2C phosphatase (*moth_1472*), which is conserved in all stressosome loci and is responsible for the dephosphorylation of RsbR and RsbS. A diguanylate cyclase follows (*moth_1471*), comprising an N-terminal, RsbU-like kinase recruitment domain, a GAF domain and the GG(D/E)EF diguanylate cyclase catalytic domain. GAF domains are often found associated with cyclic di-GMP specific phosphodiesterases (Ho et al., 2000). Diguanylate cyclases have a conserved GG(D/E)EF signature motif near the active site (Hecht and Newton, 1995; Chan et al., 2004) and synthesize the secondary messenger cyclic di-GMP from GTP (Ross et al., 1987). Cyclic di-GMP is used by a wide range of bacteria in a variety of contexts, including various signal transduction processes. For instance, cellulose synthesis is affected by cyclic di-GMP levels in *Gluconacetobacter xylinus* (Ross et al., 1987), and biofilm formation and motility in *Pseudomonas aeruginosa* are regulated by cyclic di-GMP levels (Hickman et al., 2005). In both *Vibrio cholerae* (Tischler and Camilli, 2004) and *Salmonella enterica* serovar Typhimurium (Hisert et al., 2005), reduction of cyclic di-GMP concentration results in the induction of virulence genes. Cyclic di-GMP has also been shown to interact directly with riboswitch Cd1, where a decrease in cyclic di-GMP concentration increases the level of translation of the downstream flagella operon (Sudarsan et al., 2008). The opposing, degradative activity is performed by phosphodiesterases, which are characterized by conserved amino acid motifs, in this case either EAL or HD-GYP (Tchigvintsev et al., 2010). It is common for proteins with GG(D/E)EF, EAL, or HD-GYP domains to be associated with domains that receive signals, such as the PAS domain, which is also found frequently in two-component histidine kinases.

Herein, we characterize the entire *M. thermoacetica* stressosome locus, presenting complementary structural and functional evidence for the roles of each protein in this widely adopted signaling system, which we show has been adapted by this bacterium to regulate the biosynthesis of a ubiquitous secondary messenger signaling molecule, cyclic di-GMP.

RESULTS

Moorella thermoacetica Stressosomes

The first gene in the *M. thermoacetica* stressosome operon, *moth_1475*, encodes a homolog to *B. subtilis* RsbR. However, as σ^B is not present in this operon, we have named this protein MtR (*M. thermoacetica* RsbR-like protein) hereafter. The genome of *M. thermoacetica* encodes a single RsbR-like protein; this is in contrast to *B. subtilis*, which encodes four further homologs of RsbR. MtR and *B. subtilis* RsbR share 30% overall sequence identity (12% and 53% for the N- and C-terminal domains, respectively), whereas MtS and *B. subtilis* RsbS share 38% sequence identity. The crystal structure of the N-terminal domain of MtR (Mt*N*-R) was determined to 2.0 Å resolution (Figures 1A and 1B; Table 1). Despite sharing just 12% sequence identity, the Mt*N*-R structure is remarkably similar (root-mean-squared Cα deviation of 2.5 Å over 108 aligned residues) to that of the previously determined equivalent domain of RsbR from *Bacillus subtilis* (PDB ID: 2BNL) (Murray et al., 2005; Figure 1C). The crystallographic Mt*N*-R dimer interface is formed by the long C-terminal α helix, α5, which extends away from the central globin domain and consists of a number of hydrophobic residues (Phe116-Leu141) (Figure 1B). In Mt*N*-R, the C-terminal α helix, α5, is ordered for four helical turns longer than that seen in *B. subtilis N*-RsbR (Figure 1C). When docked into the

Table 1. Crystallographic Data and Refinement Statistics

	N-*Mt*R SeMet	*Mt*S-P	*Mt*S S58E	*Mt*X Halide	*Mt*X SeMet	*Mt*X Native
Data Collection						
Wavelength	0.9716	0.9760	0.9790	1.5400	0.9795	0.9804
Space group	$P\,4_322$	$P\,2_12_12_1$	$P\,2_12_12_1$	$P\,2_12_12_1$	$P\,2_12_12_1$	$P\,2_12_12_1$
Unit cell	a = 56.4	a = 50.7	a = 49.9	a = 42.1	a = 42.1	a = 42.1
	b = 56.4	b = 61.2	b = 60.8	b = 47.7	b = 47.7	b = 47.8
	c = 148.3	c = 89.5	c = 88.9	c = 87.8	c = 87.8	c = 87.2
Resolution range (Å)	52.72–2.70 (2.97–2.70)	61.0–2.87 (3.50–2.87)	49.94–1.90 (1.97–1.90)	43.76–2.50 (2.64–2.50)	47.80–3.00 (3.16–3.00)	37.88–1.75 (1.79–1.75)
Observations	37,3626 (55410)	44,374 (5,917)	78,574 (11,744)	126,207 (18,656)	18,671 (2,809)	121,619 (17,759)
Multiplicity	52.3 (55.2)	6.5 (6.2)	3.6 (3.7)	19.7 (20.5)	4.8 (5.1)	6.7 (6.9)
Anomalous multiplicity	29.4 (29.9)	—	—	10.9 (10.9)	2.7 (2.8)	—
Anomalous correlation	87. 0 (40.3)	—	—	53.7 (12.4)	6.5 (−4.2)	—
Completeness (%)	100.0 (100.0)	99.7 (99.1)	98.2 (98.9)	99.8 (99.7)	99.8 (100.0)	99.7 (100.0)
Anomalous completeness (%)	100.0 (100.0)	—	—	100.0 (99.9)	98.6 (99.1)	—
Average I/sigma I	49.2 (16.8)	20.0 (7.2)	12.2 (2.8)	23.3 (8.8)	9.9 (4.7)	10.5 (3.1)
R_{merge} (%)	7.1 (36.6)	6.7 (24.5)	5.5 (37.0)	9.5 (37.0)	12.5 (32.2)	7.2 (34.1)
R_{anom} (%)	2.9 (5.4)	—	—	3.7 (9.5)	7.0 (2.7)	—
Refinement						
Resolution range (Å)	52.75–2.70 (2.97–2.70)	44.52–2.87 (3.03–2.87)	49.94–1.90 (2.0–1.90)	—	—	29.48–1.75 (1.84–1.75)
Reflections	12,435 (3,055)	6,777 (959)	21,867 (3,164)	—	—	18,067 (2,519)
R_{work}	0.214 (0.282)	0.211 (0.256)	0.192 (0.294)	—	—	0.152 (0.176)
R_{free}	0.275 (0.384)	0.273 (0.33)	0.240 (0.308)	—	—	0.189 (0.191)
Number of protein atoms	1,113	1,763	1,824	—	—	1,516
Number of solvent atoms	6	25	169	—	—	151
Rmsd						0.016
Bond lengths (Å)	1.512	0.004	0.008	—	—	
Bond angles (°)	0.734	0.908	1.032	—	—	
Ramachandran						
Favored (%)	97.8	92.9	97.7	—	—	98.5
Allowed (%)	2.2	6.1	2.3	—	—	1.5
B factors						
Wilson B $Å^2$	56.7	42.9	30.5	—	—	19.3
Average B factor $Å^2$	68.8	48.1	38.6	—	—	29.0
PDB id	3ZTA	3ZTB	3ZXN	—	—	3ZT9

Values in parentheses are for highest resolution shell.

B. subtilis stressosome cryo-EM envelope, this pair of α helices in the Mt*N*-R dimer extend perfectly into the neck region between the peripheral "turrets" and the core of the stressosome (Figure 1D), demonstrating that the crystallographic dimer is the biological form within the stressosome. Based on this docking, helix α5 can be seen to extend into the C-terminal STAS domain, helping to position both the sensory domains, and the switch kinase, above the core of the stressosome (Figure 1E, inset) Structural rearrangements of the stressosome core during the signal transduction process are thus likely to be mediated by this α helix (Marles-Wright et al., 2008). The α5 helix is also structurally equivalent to the "J" helix of the LOV domain of *B. subtilis* YtvA, a paralog of *B. subtilis* RsbR, which regulates the response to blue light (Avila-Pérez et al., 2006; Gaidenko et al., 2006). In the case of YtvA, it has been suggested that the "J" helix plays an important role in signal transduction (Möglich and Moffat, 2007).

The *M. thermoacetica* RsbS equivalent is encoded by *moth_1474* and is referred to herein as MtS (*M. thermoacetica* RsbS-like protein). Coexpression of MtS and full-length MtR leads to the formation of stressosome-like complexes that appear to be morphologically indistinguishable to those of *B. subtilis* (Chen et al., 2003; Marles-Wright et al., 2008 and Figure 1E, inset) when visualized by TEM of negatively stained samples (Figure 1E). *M. thermoacetica* stressosomes display a more marked tendency to aggregate than their *B. subtilis*

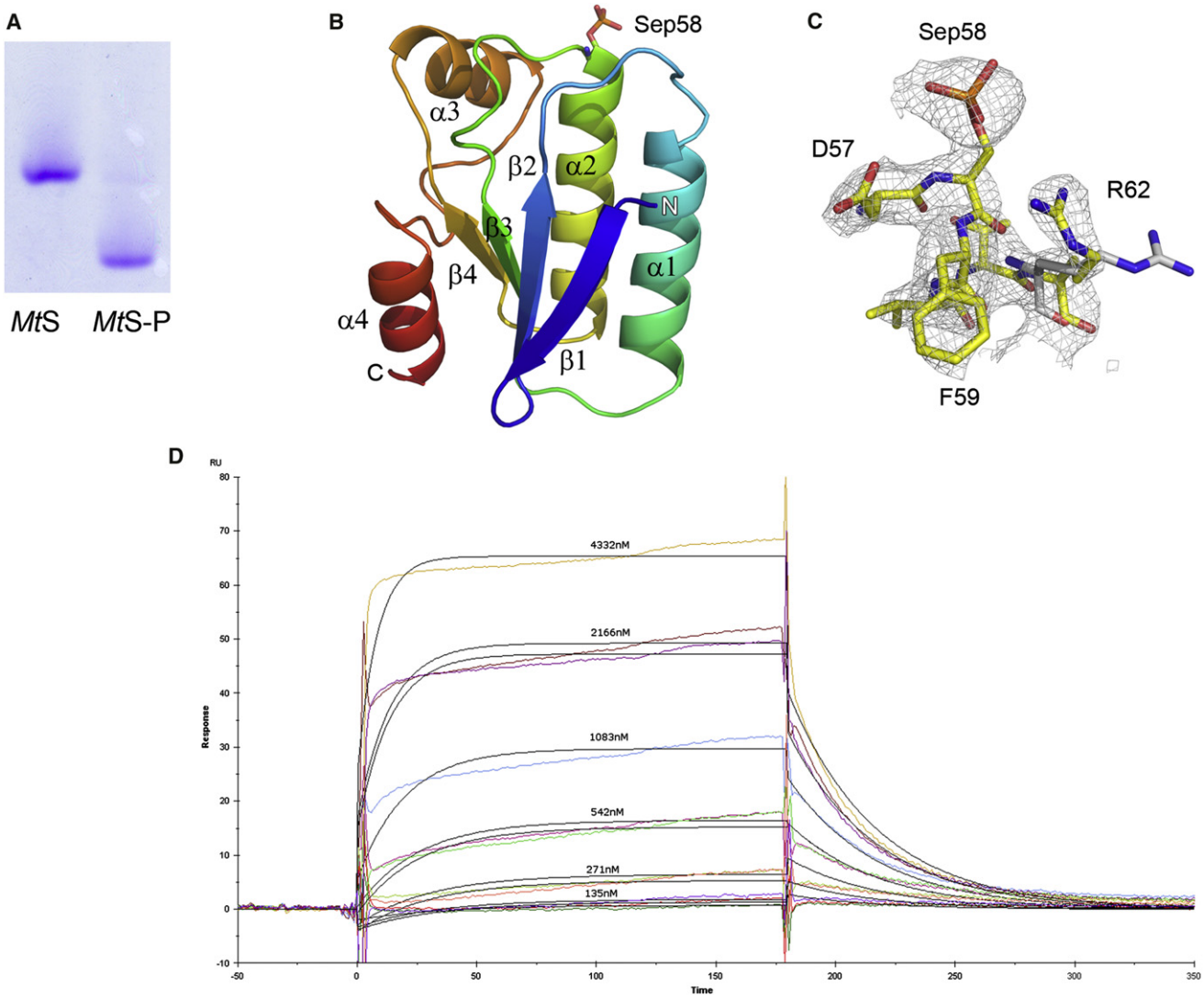

Figure 2. Phosphorylation of MtS by MtT

(A) Nondenaturing PAGE of MtS and MtS-P generated by incubation with MtT and ATP reveals a distinct band shift due to the increased negative charge of MtS-P.

(B) Cartoon of the overall fold of MtS-P with the phosphorylated Serine 58 shown as stick representation, color ramped as in Figure 1.

(C) Experimental 2mFo-DFc electron density for the phosphate accepting region of MtS, map is shown at 1 σ in gray and protein as sticks. The position of residue R62 from the second monomer in the asymmetric unit is depicted with gray carbon atoms.

(D) Interaction of immobilized MtS with various concentrations of MtT as measured by SPR. The duplicate color lines represent the measured response units and the black lines the calculated fit using 1:1 Langmuir binding model, producing calculated constants of k_a 2.63 ± 0.05 × 10^4 M^{-1} s^{-1}, k_d 2.75 ± 0.03 × 10^{-2} s^{-1}, K_D 1 × 10^{-6} M and chi^2 3.27.

counterparts (Chen et al., 2003), limiting their use for high-resolution single particle analysis of frozen, hydrated samples. Nonetheless, only *B. subtilis* stressosomes have been visualized before, and our electron micrographs (Figure 1E) are, to our knowledge, the first demonstration that stressosomes exist in organisms other than *B. subtilis* (Chen et al., 2003; Marles-Wright et al., 2008).

MtT Is a Kinase toward MtS

Since *M. thermoacetica* stressosomes proved especially prone to aggregation, and we were unable to produce soluble MtR in isolation, the role of the *M. thermoacetica* RsbT-like kinase (MtT) (encoded by *moth_1473*) was investigated using MtS as the substrate for phosphorylation. Based upon sequence alignments with other characterized STAS domains, the phosphorylation site of MtS was expected to be Ser58. Native gel electrophoresis of MtS following incubation with MtT in the presence of ATP showed that MtS was phosphorylated by MtT, with a distinct band shift observed between MtS and MtS-P as a consequence of the increased negative charge of the phosphorylated protein (Figure 2A). The phosphorylation of MtS was confirmed by mass spectroscopy, which identified a major peak in the MtS-P sample with a mass difference of 80 Da in comparison to the native protein, corresponding to

Table 2. Kinetic Parameters for MtX with *p*NPP as a Substrate

Substrate/Metal Ion	k_{cat} (s^{-1})	K_m (mM)	k_{cat}/K_m (M^{-1} s^{-1})
*p*NPP/Mn^{2+}	0.17 ± 0.01	2.56 ± 0.02	65 ± 4.95
*p*NPP/Mg^{2+}	$2.00 \times 10^{-3} \pm 8.00 \times 10^{-4}$	52.63 ± 13.68	$0.33 \times 10^{-3} \pm 7.00 \times 10^{-4}$

the addition of a single phosphate group. In order to determine the identity of the phosphorylated residue, MtS-P was subjected to LC-MS-MS following trypsin digestion, which revealed that the phosphorylation event occurred between residues 44 and 63 of MtS. This peptide, with the sequence KGLVIDISALEVV DSFVTRV, contains the predicted phosphorylation site, Ser58 (underlined), and single additional serine and threonine residues.

Structure of MtS-P

As the phosphopeptide identified by LC-MS-MS contained one threonine and two serine residues, the exact identity of the phosphorylated amino acid was determined by solving the crystal structure of MtS-P to 2.9 Å resolution (Figures 2B and 2C; Table 1), confirming that Ser58 is the recipient of the phosphoryl group from MtT (Figures 2B and 2C). The final model contains residues 6–117 in two chains and has been refined to R_{work} and R_{free} values of 0.210 and 0.273, respectively. The overall fold of the MtS-P STAS domain is essentially identical to that of the unphosphorylated MtS (Quin et al., 2008) (PDB ID: 2VY9). The two structures superimpose with an overall root-mean-squared Cα deviation of 0.4 Å with few differences in side-chain geometry. Two 8 σ peaks in the electron density adjacent to Leu98-Arg99 in one chain and the side chain of Asn106 in an adjacent chain, and between Leu103-Ala104-Leu105 from two symmetry related chains have been modeled as iodine ions due to the inclusion of sodium iodide in the crystallization conditions of MtS-P.

The electron density maps also revealed that both Ser58 residues in the crystallographic asymmetric unit could be modeled as phosphoserines (Figure 2C) with unit occupancy and B factors comparable to the adjacent amino acids. Ser58 is situated at the N terminus of helix α3, and its side chain points toward the solvent. In the nonphosphorylated form, Ser58 is not involved in any interactions with other residues, leaving it in an accessible position for enzyme-catalyzed phosphorylation and dephosphorylation reactions. In the context of the stressosome, Ser58 is situated on the external face of the complex, in a position accessible to both kinases and phosphatases (Marles-Wright et al., 2008).

To examine the implications of the phosphorylation of MtS, we investigated the interaction between MtT and MtS by surface plasmon resonance (SPR). The K_D of this interaction was determined to be 1.0 μM with a simple 1:1 Langmuir binding model (Figure 2D). It is not known how this interaction may be affected by the absence of MtR, or by the formation of the stressosome, in which MtS would ordinarily be placed. The absence of other interacting components from the stressosome suggests that the measured K_D is a gross underestimate of the interactions between MtT and the stressosome complex. However, this result contrasts with *B. subtilis* in which RsbS and RsbT do not interact in the absence of RsbR (Chen et al., 2003). An MtS S58E mutant was prepared to act as a stable mimic of phosphorylated MtS to analyze the effect of phosphorylation on the interaction between MtS and MtT. SPR analysis of the interaction between the MtS S58E mutant and MtT showed no significant binding, demonstrating that phosphorylation of MtS Ser58 is likely to cause a significant decrease in the affinity of MtT for MtS. To ensure that the MtS S58E mutation had no effect on the structure of MtS, the crystal structure was determined to 1.8 Å resolution, and revealed no significant changes in the overall architecture of the protein (see Supplemental Information available online). We note that MtR has threonine residues (Thr166, Thr200) equivalent to *B. subtilis* RsbR Thr171 and Thr205 in its STAS domain, and conclude that MtR is likely to be subjected to the same phosphorylation by MtT as RsbR is by RsbT. Our data show that rather than structural rearrangements being responsible for the release of MtT from the stressosome, the decrease in affinity of MtT for MtS on phosphorylation leads to the release of MtT to interact with its downstream partners.

Resetting the Switch: MtX Dephosphorylates MtS-P

In order to reset this system to the resting state, with MtT bound to the stressosome, the phosphorylated residues on the stressosome must be dephosphorylated. In *B. subtilis*, RsbX catalyzes the dephosphorylation of phospho-amino acids in RsbS-P and in RsbR-P (Kang et al., 1996; Chen et al., 2004; Eymann et al., 2011). The type 2C protein phosphatase RsbX is a strongly conserved part of the stressosome operon and, by analogy to the *B. subtilis* stressosome locus, *M. thermoacetica* RsbX-like protein phosphatase (MtX) (*moth_1472*) is the most likely candidate for this role. Consequently, the activity of MtX as a phosphatase toward MtS-P was tested in the presence of various divalent cations, since the PPM family of phosphatases is metal dependent. Initial experiments using the synthetic substrate *p*NPP revealed that MtX exhibits divalent cation-dependent phosphatase activity against *p*NPP (Table 2), with ~200-fold greater activity in the presence of Mn^{2+} than Mg^{2+}. Phosphatase activity was undetectable in the absence of metal ion, or in the presence of Ca^{2+}, Ni^{2+}, Zn^{2+}, or Fe^{2+} (Figure 3A). We subsequently assessed the rate of phosphatase activity of MtX toward MtS-P, and found this to also be metal dependent (Figure 3B). Complete dephosphorylation of MtS-P by MtX required the presence of Mn^{2+}, whereas the presence of Mg^{2+} impaired the rate and final level of dephosphorylation. Little or no dephosphorylation was observed in the presence of Ca^{2+} or EDTA (Figure 3B). The different level of dephosphorylation of MtS-P by MtX seen in the presence of different cations is a reflection of the chemical requirements of the phosphorolysis reaction. The ability of MtX to dephosphorylate MtS-P in the presence of Mn^{2+} was confirmed by mass spectrometry and LC-MS-MS, which revealed a mass difference of 80 Da between phosphorylated MtS-P and dephosphorylated MtS. Ions corresponding to the phosphorylated peptide KGLVIDISALEVVDSFVTRV were not

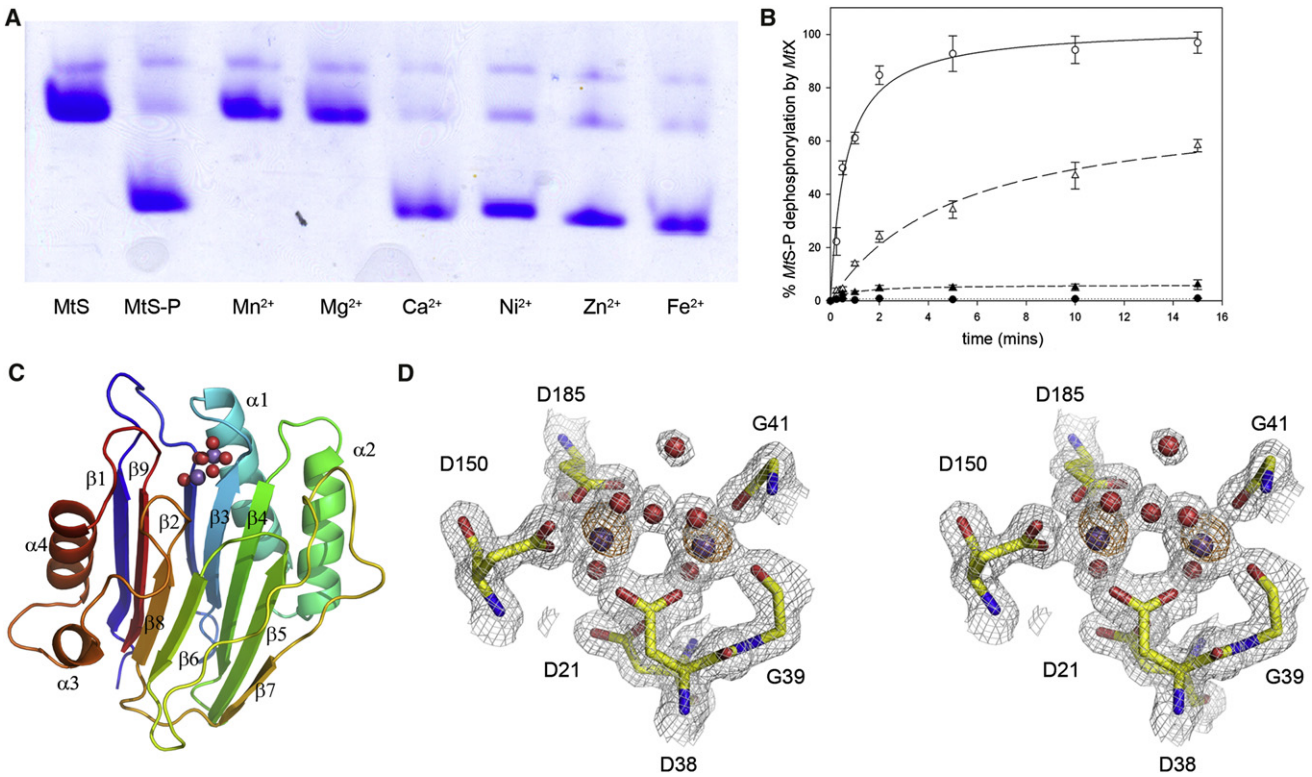

Figure 3. Metal Binding Activity of MtX and Structure of the MtX Active Site

(A) Nondenaturing PAGE gel showing the dephosphorylation of MtS-P by MtX in the presence of various divalent cations, only manganese and magnesium play a role in the reaction catalyzed by MtX (See also Table 2 for kinetic parameters with the *p*NPP substrate).

(B) Analysis of dephosphorylation efficiency over a time course by densitometry. Three replicated samples were compared for MtS-P and MtX incubated in the presence of MnCl2, MgCl2, CaCl2, and EDTA over 14 minutes at 2 minute intervals. Error bars represent 1 SD.

(C) The structure of MtX. A secondary structure cartoon is color ramped from blue to red, with Mn^{2+} ions and water molecules represented by purple and red spheres, respectively (see also Table 3 for data on structural homologs of MtX and the conservation of active site residues).

(D) Stereo view of the active site of MtX. The final refined 2mFo-DFc electron density map is shown in gray contoured at 1.5 σ around conserved active site residues. Experimental anomalous difference density for data collected at 1.54 Å is shown contoured at 5 σ in orange. Manganese ions are depicted as purple spheres and water molecules as red spheres.

observed following dephosphorylation of MtS-P by MtX, indicating that MtX hydrolyses the phosphoryl group on Ser58 of MtS-P.

Crystal Structure of MtX

To investigate the molecular mechanism by which the stressosome response is reset, we determined the crystal structure of MtX by single wavelength anomalous dispersion, and the model was refined against data to 1.75 Å resolution (Table 1). The final model comprises residues 2–193 in a single chain (Figure 3C), with crystallographic R_{work} and R_{free} values of 0.152, and 0.189, respectively.

The structure of MtX exhibits a PP2C fold (Das et al., 1996), with a central antiparallel, β sandwich of nine strands. Each face of the sandwich is flanked by pairs of antiparallel α helices (Figure 3C). Structural homologs of MtX were identified using the DALI web server (Holm and Park, 2000; Table 3). Despite relatively low sequence identity, the PP2C family displays global structural similarity. The defining member of the family, PP2Cα from *Homo sapiens* (PDB ID: 1A6Q) has an N-terminal, catalytic domain of 290 residues that is a little larger than that of MtX, with six α helices and 11 β strands (Das et al., 1996). This protein superimposes onto MtX with an root mean squared Cα deviation of 2.1 Å over 166 residues. There is a cluster of acidic residues in human PP2Cα, Asp38, Asp60, Asp239, and Asp282, which define the active site. The equivalent residues in MtX are Asp21, Asp38, Asp150, and Asp185. This cluster of acidic residues is highly conserved in prokaryotic and eukaryotic PPM phosphatases (Table 3) and is required for catalysis. Two peaks were observed at levels of 5 σ in an anomalous difference map (Figure 3D) calculated from diffraction data collected at a wavelength of 1.54 Å. The two peaks correspond to a pair of octahedrally coordinated metal ions, which were modeled as manganese due to the presence of $MnCl_2$ in the crystallization buffer. The metal ions and the acidic cluster define the active site of MtX, which is described below (see also Supplemental Information for further discussion of the MtX structure).

MtX Catalytic Site

The PPM family of phosphatases, of which PP2Cα is a subfamily member, is characterized by the requirement for divalent metal ions for activity. As with other PPM structures, the catalytic

Table 3. Structural Homologs of MtX

Protein Name	Organism	PDB Accession Code	*z* Score	Rmsd (Å)	Sequence Identity (%)	Water Coordinating	Metal Coordinating	Water Deprotonating	Substrate Binding
MtX	*Moorella thermoacetica*	3ZT9	—	—	—	Asp21	Asp38, Gly39, Asp150	Asp185	Arg13
Tppha	*Thermosynechococcus elongatus*	2J82	21.9	2.5	19	Asp18	Asp34, Gly35, Asp193	Asp231	Arg13
PstP/Ppp	*Mycobacterium tuberculosis*	1TXO	21.5	2.6	17	Asp25	Asp38, Gly39, Asp191	Asp229	Arg20
SaSTP	*Streptococcus agalacticae*	2PK0	20.8	2.8	15	Asp18	Asp36, Gly37, Asp192	Asp231	Arg13
MsPP	*Mycobacterium smegmatis*	2JFS	20.1	2.6	20	Asp22	Asp35, Gly36, Asp185	Asp223	Arg17
PPM1B	*Homo sapiens*	2P8e	18.4	2.4	15	Asp38	Asp60, Gly61, Asp243	Asp286	Asp33
PP2Cα	*Homo sapiens*	1A6Q	18.0	2.4	15	Asp38	Asp60, Gly61, Asp239	Asp282	Arg33
PP2C	*Toxoplasma gondii*	2I44	17.4	2.3	11	Asp45	Asp67, Gly68, Asp273	Asp318	Arg40

Homologs of MtX were identified in the PDB using the DALI program. The resulting *z* score, rmsd, sequence identities, and the role of the conserved residues, as determined from the crystal structures of a number of PP2C type protein phosphatases following the superimposition of these structures upon MtX are listed below.

center of MtX is located at the apex of the central β sandwich, in an aspartate rich pocket. These conserved residues are involved in the coordination of two metal ions and are also in contact with metal-bound water molecules. The two Mn^{2+} ions in MtX are in close proximity to each other, within 3.8 Å, and are stabilized by metal-oxygen bond distances in the range of 2.1–2.3 Å. The first Mn^{2+} ion is directly coordinated by three oxygen atoms: the carboxylate side chain of Asp38, and the backbone carbonyl oxygens of Gly39 and Gly41. Three water molecules complete the coordination shell (Figure 3D). The second Mn^{2+} ion is coordinated by contacts with the carboxylate side chains of three aspartic acid residues: Asp38, Asp150, and Asp185 and three water molecules (Figure 3D). Asp21 forms hydrogen bonds to two of the metal ion coordinating water molecules. A negatively charged depression on the protein surface around the active site, may provide an ideal binding site for the corresponding phosphate and Arg62 of MtS (equivalent to His204 of MtR), which project from the surface of the STAS domain.

Both metal ions in the active site of MtX share the carboxylate side chain of Asp38 and one of the water molecules for stabilization (Figure 3D). A metal ion catalyzed dephosphorylation mechanism has already been proposed for PP2Cα (Bellinzoni et al., 2007), whereby a metal ion bridging water molecule acts as a nucleophile toward the phosphorus atom and a second water molecule protonates the leaving group, in this instance a serine or threonine side chain. Given the overall similarity in structure within the PP2Cα family, and that of the coordination of the two metal ions (Bellinzoni et al., 2007; Schlicker et al., 2008), the same reaction scheme is likely to be adopted by MtX. Therefore, the water molecule that is shared by both Mn^{2+} ions in the catalytic site of MtX will most likely act as the nucleophile in the dephosphorylation of phosphorylated amino acids. In the absence of a structure of the transition state, we cannot say which of the two solvent-accessible metal-associated water molecules act as the protonating species toward the leaving group. Alternatively, a new water molecule may associate with the departing serine (or threonine) side chain. The structure of SpoIIE from *B. subtilis* reveals an unusual metal coordination with only one manganese ion bound within the active site (Levdikov et al., 2012). The structure of *B. subtilis* SpoIIE superimposes onto MtX with a root-mean-squared Cα deviation of 2.8 Å over 112 residues. Notably SpoIIE lacks the metal ion corresponding to the first manganese in the MtX structure; this may be due to the shortening of the β strand equivalent to β3 in MtX and disorder of the subsequent loop which coordinates the metal ion (residues 39–44 in MtX); however, the SpoIIE structure is a domain-swapped dimer, the formation of which may affect the binding of this metal ion. This suggests that despite a high level of structural conservation in the core of PP2C, the exact reaction mechanism employed by different members of the family will be distinct due to significant differences in the coordination of the catalytically essential metal ions. Indeed, the shortening of this loop in SpoIIE explains why only two metal ions are bound by MtX, whereas in other PP2C structures (Pullen et al., 2004; Bellinzoni et al., 2007; Rantanen et al., 2007; Wehenkel et al., 2007; Schlicker et al., 2008) this loop is longer and three metal ions appear to be required for substrate recognition and/or the dephosphorylation reaction.

MtG Is a Diguanylate Cyclase

The final gene (*moth_1471*) in the *M. thermoacetica* stressosome operon, which we have termed MtG (*M. thermoacetica* GGEEF), encodes a predicted diguanylate cyclase. MtG comprises an N-terminal RsbU-like kinase recruitment domain, a GAF type small-molecule binding domain, and a domain with a canonical GGEEF sequence motif. Anion exchange chromatography was used to separate the substrates and reaction products produced by MtG after incubation with GTP. It has previously been demonstrated that clear separation of GMP, GDP, GTP, and cyclic di-GMP can be achieved by this procedure using the *Escherichia*

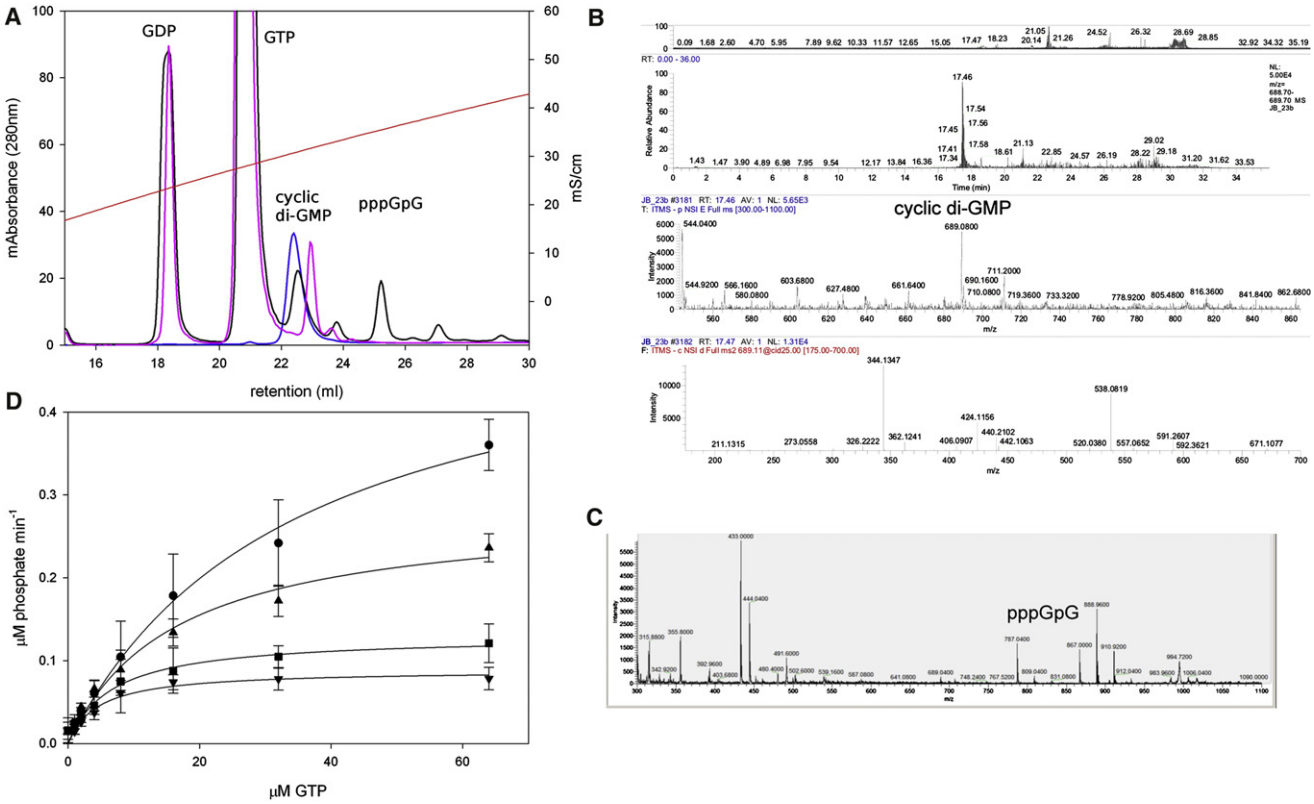

Figure 4. Reaction Products of MtG and YdeH

(A) Overlay of chromatographic spectra resulting from anion exchange of GTP (pink), overnight incubation of YdeH with GTP (blue), overnight incubation of MtG with GTP (black). The red trace represents the conductivity measured in mS/cm. The reaction of YdeH and GTP had proceeded to completion, producing cyclic di-GMP and is shown here to demonstrate where cyclic di-GMP runs on this chromatograph. MtG incubation with GTP did not proceed to completion with GTP, cyclic di-GMP and the product of a single GTP-GTP condensation reaction (pppGpG) present. The GDP present in the traces is a contamination of the GTP used in these reactions.

(B and C) Mass spectrometry of the MtG reaction products. LC-MS-MS spectra of (B) cyclic di-GMP and (C) pppGpG MtG reaction products. The peaks corresponding to the reaction products are highlighted on the individual panels.

(D) Inhibition of MtG by cyclic di-GMP. Rate of phosphate released by 0.25 μM MtG turning over GTP with the addition of: 0 μM (●); 0. 5 μM (▲); 0.75 μM (■); and 1.5 μM (▼) cyclic di-GMP to the reaction. Data are averages of four measurements and error bars represent one standard deviation. Curves were calculated using nonlinear regression in Sigmaplot.

See also Figure S1.

coli diguanylate cyclase YdeH (Zähringer et al., 2011). Following incubation of MtG and GTP, we observed a peak in the anion exchange chromatogram equivalent to the product of the YdeH reaction (Figure 4A). MALDI-TOF mass spectroscopy confirmed this peak to have a mass of 689.08 Da (Figure 4B), which corresponds to cyclic di-GMP (formula mass of 690.09 Da), thus confirming that MtG is indeed a diguanylate cyclase. An additional peak was observed on the chromatogram that eluted later than cyclic-di-GMP. This species was analyzed by MALDI-TOF mass spectroscopy, revealing a species of mass 867 Da (Figure 4C), which is consistent with that expected for pppGpG (868 Da) and comparative 1D NMR spectra of this compound and cyclic di-GMP was consistent with this assignment. pppGpG is a reaction intermediate which is formed when only one of the two condensation reactions have occurred that are required to convert two molecules of GTP into one molecule of cyclic di-GMP (Ross et al., 1987). Furthermore, the reaction catalyzed by MtG does not proceed to completion. Instead, the reaction rate of MtG decreased with increased substrate concentration, and thus MtG, like most other characterized diguanylate cyclases (Chan et al., 2004; De et al., 2009), is product inhibited. Analysis of this inhibition suggested that it is mixed, represented by a decrease in both V_{max} and K_m with increasing concentration of cyclic di-GMP, resulting in K_i values of 4 μM for competitive K_i and 0.7 μM for noncompetitive K_i (Figure 4D; Table 4). MtGAF-GGEEF was also product inhibited, with comparable K_i values (K_{ic} of 1 μM and a K_{inc} of 0.5 μM), confirming that the absence of the kinase recruitment domain has little impact on the enzymology of MtG. The competitive and noncompetitive inhibition is consistent with MtG having an I site separated spatially from the active site of the enzyme. The presence of a separate I site has been observed in other diguanylate cyclases including PleD from *Caulobacter crescentus* (Wassmann et al., 2007), and WspR from *Pseudomonas aeruginosa* (De et al., 2008) and from *Pseudomonas syringae* (De et al., 2009), the structures of which have been determined with cyclic

Table 4. Representative Kinetic Data for MtG Inhibition by Cyclic di-GMP

μM Cyclic di-GMP	V_{max}	K_m
0	0.54 ± 0.05	34.3 ± 7.3
0.5	0.28 ± 0.02	16.4 ± 2.2
0.75	0.13 ± 0.01	6.6 ± 1.8
1.5	0.09 ± 0.01	4.5 ± 0.9

V_{max} and K_m values calculated from the nonlinear regression curves shown in Figure 4D.

di-GMP bound in the I site. Sequence alignment of the GG(D/E)EF domains of *C. crescentus* PleD and WspR from *P. aeruginosa* and *P. syringae*, with MtG reveals sequence identity in this domain of around 40% (38%, 44%, and 42%, respectively) with both the I site and active site conserved between these proteins, suggesting MtG has an I site similar to both PleD and WspR (see Figure S1, related to Figure 4). Analysis of the genome of *M. thermoacetica* suggests that there are five other putative diguanylate cyclases present, three of which contain a conserved I site (Figure S1). However, the diguanylate cyclase activity of these proteins has not been confirmed experimentally.

MtT Interacts with the N-Terminal Domain of MtG

Using a nickel-affinity pull-down, His_6-MtG was found to coelute with untagged MtT (Figure 5A). When the interaction experiment was repeated with a His_6-tagged construct of MtG lacking the N-terminal domain (MtGAF-GGEEF), MtT, and MtGAF-GGEEF did not copurify (Figure 5C), suggesting that MtT interacts with the N-terminal RsbU like domain in MtG. Furthermore, the interaction of MtT with the N-terminal domain of MtG was confirmed by nondenaturing PAGE (Figure 5D). Kinetic analysis of the full-length MtG revealed a K_m of 30 μM and a k_{cat} of 0.015 s^{-1} for the turnover of GTP; the equivalent parameters for the construct lacking the N-terminal domain, MtGAF-GGEEF are 10 μM and 0.005 s^{-1}, respectively, demonstrating that the MtGAF-GGEEF domain was folded correctly and fully active in the absence of the kinase recruitment domain. SPR analysis of the strength of the interaction between MtT and full-length MtG yielded a K_D of 2 nM when analyzed with a simple 1:1 Langmuir binding model, which also revealed a slow off rate (k_d 1.80 ± 0.03 × 10^{-5} s^{-1}) (Figure 5E). This slow off rate makes accurate determination of the binding parameters nontrivial and may explain the high chi^2 observed during analysis of the data.

MtT Attenuates the Activity of MtG

When increasing amounts of MtT were incubated with MtG, a concomitant decrease in cyclic di-GMP production was observed (Figure 5F). A 25% decrease in cyclic di-GMP production was observed in the presence of 1.5-fold molar equivalents of MtT, whereas a 40% decrease was observed in the presence of a 6-fold molar equivalent of MtT. These experiments were conducted over a period of time (1 hr) chosen to maximize the amount of cyclic di-GMP produced, but still remain within the exponential phase of the reaction. When increasing concentrations of MtT were added to MtGAF-GGEEF, no change in the inhibition of cyclic di-GMP production was observed, demonstrating not only that MtT interacts with the N-terminal kinase recruitment-like domain of MtG but also that this interaction inhibits the enzyme activity of MtG. No evidence for phosphorylation of MtG by MtT was observed despite the N-terminal kinase recruitment domain containing six serines and one threonine residue. The physical interaction between MtT and MtG therefore appears to be sufficient to inhibit MtG; this observation contrasts with the stimulation of the phosphatase activity of RsbU by RsbT in the *B. subtilis* stressosome module (Yang et al., 1996) and shows that partner switching can have inhibitory as well as stimulatory effects. The molecular bases of the inhibitory effect of MtT on MtG and any effect this interaction may have on the inhibition of MtG by cyclic di-GMP was not determined. Moreover, the basis of the stimulatory effect of *B. subtilis* RsbT on RsbU remains unknown. These data demonstrate that large macromolecular assemblies, such as stressosomes, can be utilized to regulate the biosynthesis of small, secondary messenger signaling molecules.

DISCUSSION

Herein, we have presented the characterization of the entire *M. thermoacetica* stressosome signaling system. The data revealed that the proteins of the MtRST module in *M. thermoacetica* behave in a similar fashion to those of the RsbRST stressosome of *B. subtilis* (Chen et al., 2003; Kuo et al., 2004), forming a large macromolecular complex similar to that observed with *B. subtilis* RsbRST. The *M. thermoacetica* stressosomes, at least to the level afforded by TEM of negatively stained samples (Figure 1E), have the same construction as those from *B. subtilis* (Chen et al., 2003; Marles-Wright et al., 2008; Figure 1E, inset). The similarity in architecture of the stressosomes is underlined by the close structural homology of the N-terminal domains of RsbR (Murray et al., 2005) and MtR, which share little meaningful sequence identity (12%), yet both display the same nonhemeglobin fold (root-mean-squared Cα deviation of 2.5 Å over 108 aligned residues) and both form equivalent dimers (Figure 1C). Consequently, the crystal structure of the Mt*N*-R dimer fits as well to the molecular envelope of the *B. subtilis* stressosome as the equivalent dimer from the cognate RsbR (Marles-Wright et al., 2008; Figure 1D). The structure of the Mt*N*-R domain does not give further insight into the nature of the activating signal for this cascade, just as the molecular mechanism by which the *B. subtilis* stressosome responds to stress remains unknown.

The nonhemeglobin fold exhibited by *N*-RsbR and Mt*N*-R has also been observed recently in structural studies of two *Bacillus anthracis* sporulation inhibitory proteins, pXO1-118 and pXO2-61 (Stranzl et al., 2001), which titrate environmental molecules (fatty acids) that can encourage sporulation. The observed dimer interface is equivalent in all four structures of nonhemeglobin domains, and dimerization appears linked to undecanoic acid binding by the sporulation inhibitory proteins (Stranzl et al., 2011). The same dimer interface is utilized in the globin-coupled aerotaxis sensor HemAT to drive the expected piston-like signal transduction mechanism (Zhang and Phillips, 2003). Hence, the nonhemeglobin domain is an emerging and highly specific molecular sensor, the dimerization of which is likely to have a physiological role in a variety of signaling contexts.

As in the *B. subtilis* system, MtT acts as a kinase toward the STAS domain protein MtS, phosphorylating the conserved Ser58 (Figures 2A–2C). The affinity of MtT for MtS is dramatically decreased following phosphorylation of MtS by MtT, implying phosphorylation of MtS leads to the release of MtT from the MtRS stressosome complex. Our structural analysis has shown that this occurs by a mechanism based on decreased affinity for the phosphorylated form of the protein, rather than structural rearrangements caused by the phosphorylation of MtS. To reset the switch in this signaling pathway, MtS-P is dephosphorylated by MtX, allowing MtT to re-bind *M. thermoacetica* stressosomes. The presence of an MtX homolog in all stressosome operons indicates that there is an absolute necessity for a specific phosphatase to reset this pathway. *M. thermoacetica* encodes two other PP2C type proteins, *Moth_0103* and *Moth_0392*, the former is related to the SpoIIE protein of *B. subtilis*, the structure of the catalytic domain of which has been recently determined (Levdikov et al., 2012). *Moth_0103* and *Moth_0392* share only modest sequence identity (~20% in the PP2C domain) with MtX and they are thus unlikely to dephosphorylate the stressosome; structural comparisons may reveal the molecular basis of this strong substrate specificity.

The control mechanism that underpins the signal transduction processes that the stressosome regulates is called partner switching. The stressosome in *B. subtilis* regulated one of two partner switching schemes that coordinate the activity of the alternative sigma factor, σ^B, which governs the response of this bacterium to environmental stress (Boylan et al., 1993). The transition between binding partners occurs as a consequence of the phosphorylation status of the STAS domain in the system. When the STAS domain is not phosphorylated, it binds the switch kinase (Alper et al., 1994). When the STAS domain becomes phosphorylated, the switch kinase disassociates and binds the alternative partner, be that a sigma factor, a phosphatase (Yang et al., 1996), or a diguanylate cyclase as reported here. The implication of this switching behavior is that the affinity of the kinase for the nonphosphorylated STAS domain must be higher than the alternative partner, and this balance is reversed when the STAS domain is phosphorylated. The equilibrium disassociation constants measured here reveal that MtT interacts more strongly with MtG than with MtS. The slow rate of dissociation of MtT from MtG may indicate that the signaling outcome is long lasting, unlike the transient *B. subtilis* σ^B response. However, the MtS:MtT K_D is likely to be a significant underestimation as it was measured in isolation, not in the context of the stressosome where MtT will also likely interact with MtR. Analysis of recombinant, core *B. subtilis* stressosomes comprising the STAS domains of RsbR and RsbS, but lacking the N-terminal domains of RsbR shows that they do not sequester RsbT (Marles-Wright et al., 2008), indicating that in the case of *B. subtilis* contact is made between the N-terminal domain of RsbR and the kinase (Murray et al., 2005). Structural similarity between the *B. subtilis* stressosome proteins and those presented here suggest that this may also be the case for *M. thermoacetica*. Furthermore, we have been unable to obtain an estimate of the affinity of MtS-P for MtT using the S58E phosphorylation mimic of MtS, presumably because the introduction of negative charge at position 58 position reduces the affinity of MtT for MtS by several orders of magnitude, beyond the range measurable by SPR.

The partner switching pathway of *M. thermoacetica* described here is not involved in the regulation of transcription, but instead regulates the biosynthesis of the ubiquitous secondary messenger, cyclic di-GMP (Schirmer and Jenal, 2009) by exerting an inhibitory effect on the GG(D/E)EF-type diguanylate cyclase, MtG. This interaction between MtT and MtG may be stronger in vivo, or could be mediated by some as yet undetermined mechanism involving other factors not present in our analysis. GG(D/E)EF diguanylate cyclases are usually multidomain proteins that are characterized by a great variation in domain architecture beyond the conserved catalytic domain. Five other such diguanylate cyclases exist in *M. theromoacetica* (ORFs *moth_0223*, *moth_0689*, *moth_2151*, *moth_2149*, and *moth_0521*, although *moth_0521* lacks key aspects of sequence conservation in the GG(D/E)EF domain) these display significant sequence identity to MtG in the catalytic domain only, which include the active site and regulatory I site. Sequence identity in the GAF and kinase recruitment domains is, however, not maintained (see Figure S1A related to Figure 4), providing an opportunity for unique regulatory mechanisms for each diguanylate cyclase. Indeed, we have shown that MtT inhibits MtG specifically through interaction with the N-terminal kinase recruitment domain in MtG. The need for multiple control systems for cyclic di-GMP synthesizing enzymes is necessary because bacteria tend to encode several diguanylate cyclases in their genomes. For instance, sequence analysis suggests there are 3 GG(D/E)EF diguanylate cyclases in *Bacillus subtilis*, 9 in *Caulobacter crescentus*, 10 in *Escherichia coli*, and at least 25 in *Pseudomonas aeruginosa*, and presumably each is involved in a discrete process. Though individual GG(D/E)EF-diguanylate cyclases have been shown to regulate adaptive responses such as biofilm formation, chemotaxis, and virulence in bacteria such as those listed above (Jenal, 2004; Jenal and Malone, 2006), the physiological response that accompanies the stressosome-regulated cyclic di-GMP biosynthesis in *M. thermocetica* remains unknown, in part because of the absence of an established genetic system for this bacterium and the lack of simple growth conditions for this thermophilic acetogen. No physiological clues come from the genes upstream and downstream of the *M. thermoacetica* stressosome operon to indicate the wider role of these proteins.

The adoption of the stressosome as a signaling module, in both Gram-positive and negative bacteria, shows the utility of this system for mediating the response to various intracellular signals (Pané-Farré et al., 2005). The modular nature of this system allows different input domains to be coupled to various effectors through a biological signaling circuit that is responsive to the level of signal perceived and is resettable through reversible protein phosphorylation. The remarkable array of sensors that can be used in the stressosome system is exemplified by the blue-light responsive, LOV domain-containing YtvA in *B. subtilis* and the aero- or redox-sensitive, true hemoglobin sensory domains in a number of bacteria, including the pathogen, *Vibrio vulnificus* (Pané-Farré et al., 2005). The specific signals and biological responses mediated by these stressosomes remain to be determined. The question of how signaling occurs through the various sensory domains coupled to the

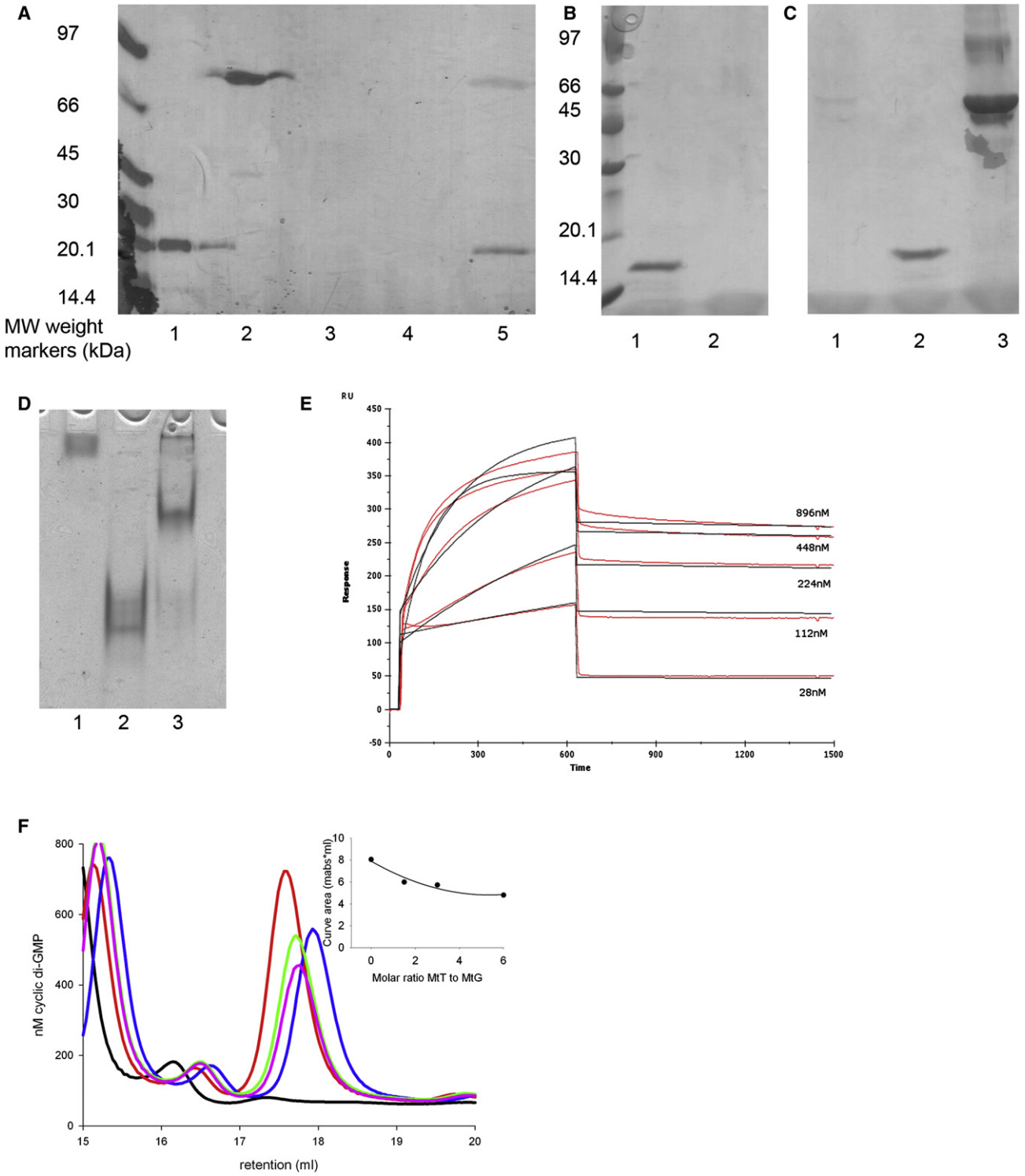

Figure 5. Interaction of MtT with MtG

(A–C) SDS PAGE gels (A-C) of Ni-NTA pull down experiments in which MtT interactions with either (A) full length His_6-MtG, (B) control with no other protein (C) the His_6-GAF-GGEEF domain of MtG were detected. (A) lane 1 and 2, purified MtT and MtG standards, respectively; lane 3, eluate after applying His_6-MtG; lane 4, eluate following subsequent addition of MtT; lane 5, bound protein eluted from the resin containing both MtT and MtG, indicating an interaction between the proteins (B) control experiment to confirm MtT does not bind to a Ni-NTA column. Lane 1, eluate following addition of MtT; lane 2, bound protein eluted from the resin, demonstrating MtT does not bind to Ni-NTA resin; (C) experiment to determine MtT binding to His_6-GAF-GGEEF. Lane 1, eluate following addition of His_6-GAF-GGEEF; lane 2, eluate after subsequent application MtT; lane 3, bound protein eluted from the resin. No MtT was observed to coelute with His_6-GAF-GGEEF suggesting no interaction.

stressosome will be resolved when activating ligands are identified in individual systems. That the stressosome has been put to use in a wide number of species from different niches shows its general utility as a tunable switching circuit that allows bacteria to respond to varied signals through the implementation of modular sensors and effectors.

EXPERIMENTAL PROCEDURES

Additional Experimental Procedures can be found in the Supplemental Information available online.

Cloning and Protein Expression

The expression plasmids for use in this study were generated from genomic DNA, amplified and cloned into pET vectors from Novagen, unless otherwise specified. For protein expression, plasmids were transformed into chemically competent *Escherichia coli* B strains and induced with IPTG for either 3–4 hr at 37°C or for 16 hr at 18°C. All cells were harvested by centrifugation and lysed by sonication after suspension in buffers appropriate for the subsequent purification.

Protein Purification

The *M. thermoacetica* proteins were purified to electrophoretic homogeneity by either a combination of nickel-NTA and size exclusion chromatography for those proteins that were His_6-tagged, or by anion or cation exchange and size exclusion chromatography for those proteins that were untagged. GST-tagged MtT was also purified by use of glutathione affinity chromatography.

Phosphorylation of MtS by MtT

MtS-P was prepared by overnight incubation of MtS with MtT in a reaction buffer containing ATP before purification by ion exchange chromatography.

Dephosphorylation of MtS-P by MtX

Dephosphorylation activity analysis was carried out by incubating the two proteins for a defined length of time, before their separation by native gel electrophoresis and analysis by densitometry.

Surface Plasmon Resonance

SPR experiments were carried out using a BIAcore 2000 or a BIAcore X-100 (BIAcore, Uppsala, Sweden) and with proteins immobilized on a CM5 chip by amine coupling. Target proteins were flowed over the surface of the chip for 1 min at a flow rate of 30 μl/min in 20 mM HEPES.NaOH (pH 7.0), 200 mM NaCl, 0.005% Tween 20. All data were analyzed using the BIAevalution software (BIAcore, Uppsala, Sweden). The reliability of the fit of the data to the model was measured according to χ^2 values.

Kinetic Experiments

MtX phosphatase assays were performed in triplicate with the substrate *p*-nitrophenyl phosphate (*p*NPP) (Sigma Aldrich). K_m and K_{cat} were calculated from Lineweaver-Burke plots. The malachite green assay was the basis for determining the rate of inorganic phosphate release from reactions including MtT and MtG.

Identification of MtG Reaction Products and Role of MtT in This Reaction

A modified version of the method used by Zähringer et al. (2011) was used to separate the nucleotides produced by MtT and MtG by anion exchange.

X-ray Crystallography

Data were collected at the Diamond Light Source and the European Synchrotron Radiation Facility, integrated using iMosflm (Leslie, 2006), or XDS (Kabsch, 2010), and scaled and merged using SCALA (Evans, 2006). The structures of MtX and N-MtR were solved by single wavelength anomalous dispersion procedures using iodine and selenium as anomalous scatterers, respectively. Heavy atom positions were located and phases were determined using SHELXC/D/E (Sheldrick, 2010). The structure of MtS-P was solved by molecular replacement using Phaser (McCoy et al., 2007) with MtS (PDB ID: 2VY9) as the search model. All structures were subjected to iterative cycles of manual fitting with COOT (Emsley et al., 2010) and refinement with Phenix.-Refine (Adams et al., 2010) until convergence. All data collection and refinement statistics are shown in Table 1.

ACCESSION NUMBERS

The atomic coordinates and structure factors have been deposited in the Protein Data Bank (http://www.ebi.ac.uk/pdbe) (PDB ID codes: Mt*N*-R, 3ZTA; MtS-P, 3ZTB; MtX, 3ZT9; MtS S58E, 3ZXN)

SUPPLEMENTAL INFORMATION

Supplemental Information includes one figure, Supplemental Results, and Supplemental Experimental Procedures and can be found with this article online at doi:10.1016/j.str.2012.01.003.

ACKNOWLEDGMENTS

This work was supported by grants from the BBSRC (BBG001553 and BBF001533). We would like to thank Dr. S. Ragsdale for the kind gift of *M. thermoacetica* genomic DNA and Dr. T. Schirmer for the kind gift of an expression plasmid containing *E. coli ydeH*. We thank the staff and beamline scientists at Diamond Light Source and the ESRF for their help with data collection and members of the Lewis laboratory for critical reading of the manuscript.

Received: September 6, 2011
Revised: January 4, 2012
Accepted: January 4, 2012
Published: February 7, 2012

REFERENCES

Adams, P.D., Afonine, P.V., Bunkóczi, G., Chen, V.B., Davis, I.W., Echols, N., Headd, J.J., Hung, L.W., Kapral, G.J., Grosse-Kunstleve, R.W., et al. (2010). PHENIX: a comprehensive Python-based system for macromolecular structure solution. Acta Crystallogr. D Biol. Crystallogr. *66*, 213–221.

Akbar, S., Kang, C.M., Gaidenko, T.A., and Price, C.W. (1997). Modulator protein RsbR regulates environmental signalling in the general stress pathway of *Bacillus subtilis*. Mol. Microbiol. *24*, 567–578.

Alper, S., Duncan, L., and Losick, R. (1994). An adenosine nucleotide switch controlling the activity of a cell type-specific transcription factor in *B. subtilis*. Cell *77*, 195–205.

Avila-Pérez, M., Hellingwerf, K.J., and Kort, R. (2006). Blue light activates the sigmaB-dependent stress response of *Bacillus subtilis* via YtvA. J. Bacteriol. *188*, 6411–6414.

(D) N-MtG:MtT nondenaturing PAGE; lane 1, N-MtG; lane 2, MtT; lane 3, N-MtG:MtT.
(E) Interaction by SPR of immobilized MtT and various concentrations of MtG analyte. The red lines represent the measured response units and the black lines the calculated fit using 1:1 Langmuir binding, producing calculated constants k_a 1.12 ± 0.02 × 10^4 M^{-1} s^{-1}, k_d 1.80 ± 0.03 × 10^{-5} s^{-1}, K_D 2 × 10^{-9} M and χ^2 28.2. The data show reasonable fit despite a high chi^2.
(F) Overlay of chromatographic spectra resulting from one hour incubations of GTP at room temperature with 0.8 μM MtG (red), MtG with 1.5-fold molar excess of MtT (blue), MtG with 3-fold excess of MtT (green) and MtG with 6-fold excess of MtT (pink) and GTP control in black. The inset shows the decreasing area of the cyclic di-GMP produced by MtG with increasing molar ratio of MtT to MtG.

Bellinzoni, M., Wehenkel, A., Shepard, W., and Alzari, P.M. (2007). Insights into the catalytic mechanism of PPM Ser/Thr phosphatases from the atomic resolution structures of a mycobacterial enzyme. Structure *15*, 863–872.

Boylan, S.A., Redfield, A.R., Brody, M.S., and Price, C.W. (1993). Stress-induced activation of the sigma B transcription factor of *Bacillus subtilis*. J. Bacteriol. *175*, 7931–7937.

Caffrey, D.R., Somaroo, S., Hughes, J.D., Mintseris, J., and Huang, E.S. (2004). Are protein-protein interfaces more conserved in sequence than the rest of the protein surface? Protein Sci. *13*, 190–202.

Chan, C., Paul, R., Samoray, D., Amiot, N.C., Giese, B., Jenal, U., and Schirmer, T. (2004). Structural basis of activity and allosteric control of diguanylate cyclase. Proc. Natl. Acad. Sci. USA *101*, 17084–17089.

Chen, C.C., Lewis, R.J., Harris, R., Yudkin, M.D., and Delumeau, O. (2003). A supramolecular complex in the environmental stress signalling pathway of *Bacillus subtilis*. Mol. Microbiol. *49*, 1657–1669.

Chen, C.C., Yudkin, M.D., and Delumeau, O. (2004). Phosphorylation and RsbX-dependent dephosphorylation of RsbR in the RsbR-RsbS complex of *Bacillus subtilis*. J. Bacteriol. *186*, 6830–6836.

Das, A.K., Helps, N.R., Cohen, P.T., and Barford, D. (1996). Crystal structure of the protein serine/threonine phosphatase 2C at 2.0 A resolution. EMBO J. *15*, 6798–6809.

De, N., Pirruccello, M., Krasteva, P.V., Bae, N., Raghavan, R.V., and Sondermann, H. (2008). Phosphorylation-independent regulation of the diguanylate cyclase WspR. PLoS Biol. *6*, e67.

De, N., Navarro, M.V., Raghavan, R.V., and Sondermann, H. (2009). Determinants for the activation and autoinhibition of the diguanylate cyclase response regulator WspR. J. Mol. Biol. *393*, 619–633.

Delumeau, O., Dutta, S., Brigulla, M., Kuhnke, G., Hardwick, S.W., Völker, U., Yudkin, M.D., and Lewis, R.J. (2004). Functional and structural characterization of RsbU, a stress signaling protein phosphatase 2C. J. Biol. Chem. *279*, 40927–40937.

Dufour, A., Voelker, U., Voelker, A., and Haldenwang, W.G. (1996). Relative levels and fractionation properties of Bacillus subtilis sigma(B) and its regulators during balanced growth and stress. J. Bacteriol. *178*, 3701–3709.

Emsley, P., Lohkamp, B., Scott, W.G., and Cowtan, K. (2010). Features and development of Coot. Acta Crystallogr. D Biol. Crystallogr. *66*, 486–501.

Eymann, C., Schulz, S., Gronau, K., Becher, D., Hecker, M., and Price, C.W. (2011). *In vivo* phosphorylation patterns of key stressosome proteins define a second feedback loop that limits activation of *Bacillus subtilis* σ^B. Mol. Microbiol. *80*, 798–810.

Evans, P. (2006). Scaling and assessment of data quality. Acta Crystallogr. D Biol. Crystallogr. *62*, 72–82.

Gaidenko, T.A., Yang, X., Lee, Y.M., and Price, C.W. (1999). Threonine phosphorylation of modulator protein RsbR governs its ability to regulate a serine kinase in the environmental stress signaling pathway of *Bacillus subtilis*. J. Mol. Biol. *288*, 29–39.

Gaidenko, T.A., Kim, T.J., Weigel, A.L., Brody, M.S., and Price, C.W. (2006). The blue-light receptor YtvA acts in the environmental stress signaling pathway of *Bacillus subtilis*. J. Bacteriol. *188*, 6387–6395.

Haldenwang, W.G., and Losick, R. (1979). A modified RNA polymerase transcribes a cloned gene under sporulation control in *Bacillus subtilis*. Nature *282*, 256–260.

Hecht, G.B., and Newton, A. (1995). Identification of a novel response regulator required for the swarmer-to-stalked-cell transition in *Caulobacter crescentus*. J. Bacteriol. *177*, 6223–6229.

Hickman, J.W., Tifrea, D.F., and Harwood, C.S. (2005). A chemosensory system that regulates biofilm formation through modulation of cyclic diguanylate levels. Proc. Natl. Acad. Sci. USA *102*, 14422–14427.

Hisert, K.B., MacCoss, M., Shiloh, M.U., Darwin, K.H., Singh, S., Jones, R.A., Ehrt, S., Zhang, Z., Gaffney, B.L., Gandotra, S., et al. (2005). A glutamate-alanine-leucine (EAL) domain protein of *Salmonella* controls bacterial survival in mice, antioxidant defence and killing of macrophages: role of cyclic diGMP. Mol. Microbiol. *56*, 1234–1245.

Ho, Y.S., Burden, L.M., and Hurley, J.H. (2000). Structure of the GAF domain, a ubiquitous signaling motif and a new class of cyclic GMP receptor. EMBO J. *19*, 5288–5299.

Holm, L., and Park, J. (2000). DaliLite workbench for protein structure comparison. Bioinformatics *16*, 566–567.

Horseman, M.A., and Surani, S. (2011). A comprehensive review of *Vibrio vulnificus*: an important cause of severe sepsis and skin and soft-tissue infection. Int. J. Infect. Dis. *15*, e157–e166.

Jenal, U. (2004). Cyclic di-guanosine-monophosphate comes of age: a novel secondary messenger involved in modulating cell surface structures in bacteria? Curr. Opin. Microbiol. *7*, 185–191.

Jenal, U., and Malone, J. (2006). Mechanisms of cyclic-di-GMP signaling in bacteria. Annu. Rev. Genet. *40*, 385–407.

Kabsch, W. (2010). Xds. Acta Crystallogr. D Biol. Crystallogr. *66*, 125–132.

Kang, C.M., Brody, M.S., Akbar, S., Yang, X., and Price, C.W. (1996). Homologous pairs of regulatory proteins control activity of *Bacillus subtilis* transcription factor sigma(b) in response to environmental stress. J. Bacteriol. *178*, 3846–3853.

Kuo, S., Zhang, S., Woodbury, R.L., and Haldenwang, W.G. (2004). Associations between *Bacillus subtilis* sigmaB regulators in cell extracts. Microbiology *150*, 4125–4136.

Leslie, A.G. (2006). The integration of macromolecular diffraction data. Acta Crystallogr. D Biol. Crystallogr. *62*, 48–57.

Levdikov, V.M., Blagova, E.V., Rwalings, A.E., Jameson, K., Tunaley, J., Hart, D.J., Barak, I., and Wilkinson, A.J. (2012). Structure of the phosphatase domain of the cell fate determinant SpoIIE from *Bacillus subtilis*. J. Mol. Biol. *415*, 343–358.

Marles-Wright, J., Grant, T., Delumeau, O., van Duinen, G., Firbank, S.J., Lewis, P.J., Murray, J.W., Newman, J.A., Quin, M.B., Race, P.R., et al. (2008). Molecular architecture of the "stressosome," a signal integration and transduction hub. Science *322*, 92–96.

McCoy, A.J., Grosse-Kunstleve, R.W., Adams, P.D., Winn, M.D., Storoni, L.C., and Read, R.J. (2007). Phaser crystallographic software. J. Appl. Cryst. *40*, 658–674.

Möglich, A., and Moffat, K. (2007). Structural basis for light-dependent signaling in the dimeric LOV domain of the photosensor YtvA. J. Mol. Biol. *373*, 112–126.

Murray, J.W., Delumeau, O., and Lewis, R.J. (2005). Structure of a nonheme globin in environmental stress signaling. Proc. Natl. Acad. Sci. USA *102*, 17320–17325.

Pané-Farré, J., Lewis, R.J., and Stülke, J. (2005). The RsbRST stress module in bacteria: a signalling system that may interact with different output modules. J. Mol. Microbiol. Biotechnol. *9*, 65–76.

Price, C.W., Fawcett, P., Cérémonie, H., Su, N., Murphy, C.K., and Youngman, P. (2001). Genome-wide analysis of the general stress response in *Bacillus subtilis*. Mol. Microbiol. *41*, 757–774.

Pullen, K.E., Ng, H.L., Sung, P.Y., Good, M.C., Smith, S.M., and Alber, T. (2004). An alternate conformation and a third metal in PstP/Ppp, the *M. tuberculosis* PP2C-Family Ser/Thr protein phosphatase. Structure *12*, 1947–1954.

Quin, M., Newman, J., Firbank, S., Lewis, R.J., and Marles-Wright, J. (2008). Crystallization and preliminary X-ray analysis of RsbS from *Moorella thermoacetica* at 2.5 A resolution. Acta Crystallogr. Sect. F Struct. Biol. Cryst. Commun. *64*, 196–199.

Rantanen, M.K., Lehtiö, L., Rajagopal, L., Rubens, C.E., and Goldman, A. (2007). Structure of *Streptococcus agalactiae* serine/threonine phosphatase. The subdomain conformation is coupled to the binding of a third metal ion. FEBS J. *274*, 3128–3137.

Ross, P., Weinhouse, H., Aloni, Y., Michaeli, D., Weinberger-Ohana, P., Mayer, R., Braun, S., de Vroom, E., van der Marel, G.A., van Boom, J.H., and Benziman, M. (1987). Regulation of cellulose synthesis in *Acetobacter xylinum* by cyclic diguanylic acid. Nature *325*, 279–281.

Schirmer, T., and Jenal, U. (2009). Structural and mechanistic determinants of c-di-GMP signalling. Nat. Rev. Microbiol. *7*, 724–735.

Schlicker, C., Fokina, O., Kloft, N., Grüne, T., Becker, S., Sheldrick, G.M., and Forchhammer, K. (2008). Structural analysis of the PP2C phosphatase tPphA from *Thermosynechococcus elongatus*: a flexible flap subdomain controls access to the catalytic site. J. Mol. Biol. *376*, 570–581.

Sheldrick, G.M. (2010). Experimental phasing with SHELXC/D/E: combining chain tracing with density modification. Acta Crystallogr. D Biol. Crystallogr. *66*, 479–485.

Stranzl, G.R., Santelli, E., Bankston, L.A., La Clair, C., Bobkov, A., Schwarzenbacher, R., Godzik, A., Perego, M., Grynberg, M., and Liddington, R.C. (2011). Structural insights into inhibition of *Bacillus anthracis* sporulation by a novel class of non-heme globin sensor domains. J. Biol. Chem. *286*, 8448–8458.

Sudarsan, N., Lee, E.R., Weinberg, Z., Moy, R.H., Kim, J.N., Link, K.H., and Breaker, R.R. (2008). Riboswitches in eubacteria sense the second messenger cyclic di-GMP. Science *321*, 411–413.

Tchigvintsev, A., Xu, X., Singer, A., Chang, C., Brown, G., Proudfoot, M., Cui, H., Flick, R., Anderson, W.F., Joachimiak, A., et al. (2010). Structural insight into the mechanism of c-di-GMP hydrolysis by EAL domain phosphodiesterases. J. Mol. Biol. *402*, 524–538.

Tischler, A.D., and Camilli, A. (2004). Cyclic diguanylate (c-di-GMP) regulates *Vibrio cholerae* biofilm formation. Mol. Microbiol. *53*, 857–869.

Wassmann, P., Chan, C., Paul, R., Beck, A., Heerklotz, H., Jenal, U., and Schirmer, T. (2007). Structure of BeF3- -modified response regulator PleD: implications for diguanylate cyclase activation, catalysis, and feedback inhibition. Structure *15*, 915–927.

Wehenkel, A., Bellinzoni, M., Schaeffer, F., Villarino, A., and Alzari, P.M. (2007). Structural and binding studies of the three-metal center in two mycobacterial PPM Ser/Thr protein phosphatases. J. Mol. Biol. *374*, 890–898.

Yang, X., Kang, C.M., Brody, M.S., and Price, C.W. (1996). Opposing pairs of serine protein kinases and phosphatases transmit signals of environmental stress to activate a bacterial transcription factor. Genes Dev. *10*, 2265–2275.

Zähringer, F., Massa, C., and Schirmer, T. (2011). Efficient enzymatic production of the bacterial second messenger c-di-GMP by the diguanylate cyclase YdeH from *E. coli*. Appl. Biochem. Biotechnol. *163*, 71–79.

Zhang, W., and Phillips, G.N., Jr. (2003). Structure of the oxygen sensor in *Bacillus subtilis*: signal transduction of chemotaxis by control of symmetry. Structure *11*, 1097–1110.